ISSN 0915-633X

NATIONAL INSTITUTE FOR FUSION SCIENCE

Nonlinear Incompressible Poloidal Viscosity in L=2 Heliotron and Quasi-Symmetric Stellarators

M. Yokoyama, N. Nakajima and M. Okamoto

(Received - Sep. 29, 1997)

NIFS-519 Nov. 1997

RESEARCH REPORT
NIFS Series

NAGOYA, JAPAN

Nonlinear Incompressible Poloidal Viscosity in $L = 2$ Heliotron and Quasi-Symmetric Stellarators

M.Yokoyama, N.Nakajima, M.Okamoto

National Institute for Fusion Science, Toki, 509-52, Japan

Abstract

The possibility of occurence of the L-H transition is examined in $L = 2$ heliotron and quasi-symmetric (QS) stellarators based on the nonlinear incompressible poloidal viscosity for the plateau to Pfirsch-Schlüter regime. Fourier spectra of the magnetic field strength $|B|$ in the Hamada coordinates are employed for the calculation. The appearance of the local maxima of poloidal viscosity as a function of poloidal flow velocity greatly depend on the relative amplitudes between the toroidicity and helicities in the magnetic field. Effects of magnetic configuration control such as the inward magnetic axis shift and quadrupole field control on the poloidal viscosity are investigated in the Large Helical Device (LHD)-like $L = 2$ heliotron. Finite beta effects are also briefly studied based on the fixed boundary magnetohydrodynamic (MHD) equilibria. Due to the well suppressed non-symmetric magnetic spectra in the Boozer coordinates for QS configurations, QS properties are well maintained even in the Hamada coordinates. Therefore, the single clear local maximum can be obtained for QS configurations.

KEYWORDS

nonlinear incompressible poloidal viscosity, $L = 2$ heliotron, quasi-symmetric stellarators, Boozer coordinates, Hamada coordinates, helicity induced local maximum (HM), toroidicity induced local maximum (TM)

1 Introduction

An explanation of the physical mechanisms for the occurence of L-H transition is based on the bifurcation of the radial electric field through the existence of local maxima in the poloidal viscosity as a function of the poloidal flow velocity [1, 2]. Subsequent suppression of the turbulent fluctuations is due to the $\boldsymbol{E} \times \boldsymbol{B}$ velocity shear and the diamagnetic angular velocity shear [3, 4]. Plasma poloidal viscosity is a nonlinear

function of the radial electric field and has a local maximum. The qualitative results based on this bifurcation model are in good agreement with the measurements in the L-H transition as demonstrated in several tokamaks [1, 2, 5, 6].

In the previous papers [7, 8], this bifurcation model which is extended to non-symmetric magnetic configurations was applied to several heliotron/stellarator configurations. The approximate truncated magnetic field spectra were used there to compare several heliotron/stellarator devices with different relative amplitudes between the toroidicity and helicities in the magnetic field. Therefore, the only representative configuration was considered there for the Large Helical Device (LHD) [9] which will have first experiments in the March 1998.

The LHD has a geometrical major radius of 3.9 m and consistes of 2 helical coils with 10 field periods and three pairs of poloidal coils. This coil design allows to control magnetic configuration properties in a wide range. The so-called standard configuration is optimized from the viewpoints of high beta plasmas, good energetic particle confinement and divertor operation [9]. The standard magnetic configuration has a planar magnetic axis with the major radius of 3.75 m or the magnetic axis is shifted 15 cm inward from the geometrical major radius. It is noted that the magnetic surface cross section averaged in the toroidal direction is almost circular. The dipole and/or quadrupole magnetic field control are possible with utilizing the large flexibility of the combination of coil current ratios, which contributes to vary the magnetic axis position and/or to deform the toroidal-averaged magnetic surface cross section to horizontally or vertically elongated one.

On the other hand, the concept of quasi-symmetric (QS) configurations [10, 11, 12] have been considered for the improvement of energetic particle confinement by realizing the symmetric properties for the magnetic field. It is noted that the HSX [13] is based on quasi-helically symmetric (QHS) concept. Some plasma confinement properties of quasi-axisymmetric (QAS) configurations have been reported [14, 15]. One another attractive aspect of the QS configurations would be maintaining the plasma rotation to suppress the anomalous transport due to plasma flow shear by reducing the viscous damping.

In this paper, above mentioned configurations are examined from the point of view of the nonlinear poloidal viscosity to clarify the possibility of the bifurcation of the poloidal flow velocity, which may be relevant to the L-H transition. Effects of magnetic configuration control are also investigated for the LHD, which may give a guidance for the forthcoming experiments. This paper is organized as follows. In Section 2,

the expression of the poloidal viscosity calculated in this paper is re-written from Ref. [8] and re-explained very shortly for convenience. Section 3 is devoted to explain the results for a wide variety of configurations possible in LHD-like $L = 2$ heliotron and QS configurations. Brief summary will be given in Section 4.

2 Nonlinear Incompressible Poloidal Viscosity

The bifurcation theory of poloidal rotation is employed to tokamaks as the model for the L-H transition [3]. It has been extended to stellarators/heliotrons to suggest a new set of experiments that can be performed in a controlled manner for examining this theory [7]. Based on this work, the nonlinear incompressible poloidal viscosity has been calculated to clarify the characteristics of present and next generation stellarator/heliotron devices from the L-H transition point of view. The derivation of nonlinear incompressible poloidal viscosity based on drift kinetic equations with plasma flows is described in Ref. [7]. The same notations are used in this paper. From the definition

$$\langle \boldsymbol{B}_p \cdot \nabla \cdot \boldsymbol{\Pi} \rangle = \langle \int d^3v m_A [(v^2/2) - (3v_\parallel^2/2)] f \boldsymbol{B}_p \cdot \nabla B/B \rangle \,, \tag{1}$$

and some assumptions as described in Ref. [8], the poloidal viscosity in the plateau to Pfirsch-Schlüter regime can be obtained as [7]

$$\begin{aligned} -\frac{\langle \boldsymbol{B}_p \cdot \nabla \cdot \boldsymbol{\Pi} \rangle}{N m_A v_T^2 \chi'} &= \frac{\sqrt{\pi}}{4} \sum_{mn} \epsilon_{mn}^2 m(m - nq) \\ &\times \left\{ I_{mn} \left[\frac{V_\parallel}{v_T} + \frac{m}{m - nq} (M_p - V_{p,P}) \right] - L_{mn} \frac{m}{m - nq} V_{p,T} \right\} \\ &+ \epsilon_t^2 \left(\frac{\nu_{eff}}{(v_T/qR)} \right) \left(\frac{V_\parallel}{(v_T q^2)} + 2M_p - 2V_{p,P} \right) , \end{aligned} \tag{2}$$

where $V_{p,P} = -c(dP/dr)/(Nev_T B_p)$, $V_{p,T} = -c(dT/dr)/(ev_T B_p)$, and $M_p = -cE_r/(B_p v_T)$. In obtaining eq. (2), The conversion formula is employed to express Hamada coordinates [16] in terms of standard toroidal coordinates for a tokamak [17]. Thus eq. (2) is approximate. It is noted that M_p is positive for $E_r < 0$. The second term in eq. (2) is related to the charge exchange momentum loss and $\nu_{eff} = N_n \langle \sigma v \rangle_{cx}$, where N_n is the neutral density and $\langle \sigma v \rangle_{cx}$ is the reaction rate of charge exchange reaction. The physical model of the L - H transition based on the nonlinear poloidal viscosity is explained briefly in Appendix in Ref. [8].

The three dimensional equilibrium code VMEC [18] (fixed boundary version) has been applied to calculate currentless equilibria. The pressure profile for finite beta cases is assumed as

$$P = P_0 (1 - \psi_T)^2 \,,$$

which is frequently observed in CHS [19] experiments. In Ref. [8], representative magnetic field components for several experimental devices are chosen based on the Boozer coordinates [20] to clarify the general dependence of poloidal viscosity on the magnetic field structure. However; the poloidal viscosity, eq. (2), is obtained based on the Hamada coordinates. Therefore, more accurately, magnetic field spectra in the Hamada coordinates should be used to calculate the poloidal viscosity based on eq. (2). The transformation between the Boozer and the Hamada coordinates is clarified in Ref. [21]. It is pointed out there that the magnetic field spectra in the Hamada coordinates is broader than those in the Boozer coordinates especially in the region of plasma periphery, where the poloidal viscosity is considered in this paper. This clarified transformation from the Boozer to the Hamada coordinates is utilized to obtain the magnetic field spectra in the Hamada coordinates with a sufficient accuracy.

3 Properties of Poloidal Viscosity in $L = 2$ Heliotron and quasi-symmetric Stellarators

In this section, the nonlinear poloidal viscosity is calculated for LHD-like $L = 2$ heliotron and quasi-symmetric stellarators to clarify the relationships between the magnetic field spectra in the Hamada coordinates and the poloidal plasma rotation properties.

3.1 LHD-like $L = 2$ Heliotron

The LHD has two helical coils with ten field periods and three pairs of poloidal coils. These two helical coils are designed so that each helical coil current can be controlled individually, which allows to realize spatial axis configurations [22]. Moreover, each helical coil consists of three current layers, which makes possible to vary the effective minor radius of helical coils [23]. On the other hand, three pairs of poloidal coils are utilized to control dipole and/or quadrupole and hexapole field to vary the plasma surface cross sections which influences the magnetohydrodynamic (MHD) equilibrium and stability properties. These experimental flexibility is a great advantage to investigate a wide range of magnetic configurations to approach the desirable or optimized helical systems for the future.

As described above, the LHD can produce a wide variety of magnetic configurations. Among these several configurations, the so-called standard configuration is optimized to

make compatible high beta plasmas with good energetic particle confinement by shifting the magnetic axis about 15 cm inward compared to the geometrical major radius of the device [24]. This inward magnetic axis shift strongly correlates to restore helical symmetry in the magnetic configuration. In this optimization process, the plasma rotation properties have not been taken into account. Therefore, the poloidal viscosity in typical magnetic configurations possible in the LHD are studied in this subsection, which will provide the direction to optimize LHD experiments further or make them more attractive to clarify the toroidal plasma physics.

The LHD standard-like configuration is considered to compare with the previous results shown in Ref. [8]. The poincaré plots of magnetic field lines for this configuration are shown in Fig. 1(a) at $\phi = 0, (1/4)(2\pi/10)$ and $(1/2)(2\pi/10)$, where ϕ is the geometrical toroidal angle. It is noted that the toroidal-averaged magnetic surface cross sections are almost circle. Figure 1(b) represents the Fourier spectra of magnetic field strength $|B|$ in the Boozer coordinates, and Fig. 1(c) in the Hamada coordinates both on the magnetic surface at $r/a \sim 0.98$. The magnetic field strength $|B|$ is expressed as

$$B = \sum_{mn} B_{mn}(r) \cos(m\theta - n\zeta) ,$$

where θ (ζ) is the poloidal (toroidal) angle in each coordinate system and r the label of the magnetic surface. They are normalized with the uniform magnetic field strength on that magnetic surface, that is, $\epsilon_{m,n} \equiv B_{mn}/B_{00}(r \sim 0.98a)$ are shown. It is clearly seen from Fig. 1(b) that the magnetic field spectra in the Boozer coordinates reflect the real geometry of magnetic configuration with the toroidicity $\epsilon_{1,0}$ and the helicity $\epsilon_{2,10}$. However, the helicity $\epsilon_{2,10}$ is converted to other helical components such as $\epsilon_{1,10}$ and $\epsilon_{3,10}$ due to the mode coupling in the transformation to the Hamada coordinates. This structure of the magnetic field components in the Hamada coordinates strongly deviate from the simple intuitions for the magnetic field spectra. It should be noted that the relative error of the magnetic field strength in the transformation is about 2×10^{-6} at the most between Fig. 1(b) and 1(c).

Figure 2 shows the normalized poloidal viscosity

$$\Pi_{p,n} = \langle \boldsymbol{B}_p \cdot \nabla \cdot \boldsymbol{\Pi} \rangle / (N m_i v_T^2 \chi' \sqrt{\pi}/4) \tag{3}$$

versus poloidal Mach number M_p in the LHD standard-like configuration for $V_{p,P} = 0.2, V_{p,T} = 0.1$ and $(\nu_{*i}, \nu_{eff}/(v_T/Rq)) = (1, 0.01), (1, 0.1)$ and (12, 0.01) cases. The safety factor is $q \sim 0.91$ in this case. In Ref. [25], $V_{p,P} = 0.1$ and $V_{p,T} = 0.2$ are assumed, however; effects of these choices on $\Pi_{p,n}$ is fairly weak. Figure 2 clearly shows

the fairly weak effects of plasma parameters such as effective ion-ion collision frequency (ν_{*i}) and/or neutral-ion collision frequency $\nu_{eff}/(v_T/Rq)$. Therefore, the following calculations are performed with $(\nu_{*i}, \nu_{eff}/(v_T/Rq)) = (1, 0.01)$. It is shown in Ref. [8] that the local maximum of poloidal viscosity can occur at the poloidal Mach number M_p somewhat larger than $|m-nq|/m$, where q is the safety factor. Accordingly, $\epsilon_{3,10}$ causes the local maximum around $M_p \gtrsim 2$ and $\epsilon_{1,10}$ gives it around $M_p \gtrsim 8$. Therefore, it can be said that the local maximum appearing around $M_p \sim 3$ arises from the helicity with $(m, n) = (3, 10)$. This helicity induced local maximum (HM) shades the toroidicity induced local maximum (TM) around $M_p \lesssim 2$. The curves shown in Fig. 2 with the large HM and almost shaded TM is qualitatively the same as those in Figs. 8 and 9 (used the same parameters as here) in Ref. [8]. In Ref. [8], the model magnetic field spectra similar to those in the Boozer coordinates are used to calculate $\Pi_{p,n}$, and therefore, the dominant helicity is $\epsilon_{2,10}$, which causes the local maximum around $M_p \gtrsim 3.5$. This Mach number is larger than those for above mentioned $\epsilon_{3,10}$, which makes possible to leave TM unshaded to some extent. This comparison implies that the helicity causing the local maximum at far from or too close to the TM around $M_p \gtrsim 1$ is effective to stand out the TM. The remarkable TM makes possible the bifurcation of poloidal Mach number at relatively small Mach number. It would be necessary to grasp some tendencies to control the helicities in the Hamada coordinates to vary HM to realize the remarkable TM, because the Fourier spectra of $|B|$ in the Hamada coordinates are not easy to guess from the real geometry as shown in Fig. 1(c). Therefore, several typical magnetic configurations possible with the LHD coil system are considered in the following to clarify the relationships between magnetic configuration control and poloidal rotation properties.

Figure 3 shows the poloidal plasma viscosity for three vacuum configurations with $\Delta = -30, -15$ (standard-like), and 0 cm, where Δ denotes the magnetic axis shift compared to the geometrical major radius, $R_0 = 3.9$ m. It is easily seen that the configuration with larger inward magnetic axis shift causes the less remarkable TM (around $M_p \gtrsim 1$) or more enhanced HM. Especially, the dependence of $\Pi_{p,n}$ on M_p in the configuration without inward magnetic axis shift ($\Delta = 0$ cm) is similar to that in tokamaks. For reference, six dominant magnetic field components in the Hamada coordinates are listed for these configurations in Table I. It should be noted that the toroidicity $\epsilon_{1,0}$ becomes smaller as $|\Delta|$ is increased or the magnetic axis is shifted more inward. This tendency can be understood qualitatively as follows. As well known, when the straight helical configurations are bent into the torus geometry, the magnetic axis is

shifted outward compared to its original position due to the toroidicity to maintain an equilibrium. Therefore, inward magnetic axis shift strongly correlates to restore helical symmetry with reduced toroidicity. From Fig. 3, magnetic configurations with smaller inward magnetic axis shift may be favorable from the point of views of the poloidal rotation properties, although particle orbit properties would be deteriorated compared to the standard-like configuration [9].

By utilizing the poloidal coil sets so as to control quadrupole field, magnetic surface cross sections are varied to vertically or horizontally elongated (in the toroidal average) shape. Here one example configuration which has a horizontally elongated shape in toroidal average with almost the same inward magnetic axis shift ($\Delta = -13$ cm) as the standard-like configuration is examined. Magnetic surface cross sections on three poloidal cross sections are shown in Fig. 4(a), where largely horizontally elongated cross section appears at $\phi = (1/2)(2\pi/10)$ and the vertically elongated cross section at $\phi = 0$ in the standard-like configuration (cf., Fig. 1(a)) becomes more circular one. Table II lists the five dominant magnetic field components for this configuration. As compared to the standard-like configuration with $\Delta = -15$ cm listed in the Table I, the toroidicity $\epsilon_{1,0}$ is almost the same, however; helicities causing HM around small M_p such as $\epsilon_{3,10}$ are significantly suppressed. The dominant helicity to cause HM around small M_p is $\epsilon_{4,10}$ for this case, however; it has a relatively small amplitude compared to that of $\epsilon_{3,10}$ in the standard-like case. As shown in Fig. 4(b), this $\epsilon_{4,10}$ makes HM around $M_p \gtrsim 1.2$ with smaller contribution to $\Pi_{p,n}$, which arises the broad and weak local maximum with smaller $\Pi_{p,n}$ compared to that in the standard-like configuration. For reference, the result for the vertically elongated case with $\Delta = -16$ cm is also shown in Fig. 4(b). Figure 4(b) implies that there is a possibility to control the dependence of M_p on the poloidal viscosity through the variation of plasma surface cross sections.

As for the finite beta effects on poloidal viscosity, they are examined in the standard-like configuration and shown in Fig. 5 for $\beta(0) = 0, 4$ and 8% cases with the above described pressure profile. It shows that there is only a little change among these three cases. It implies that there is little variation of magnetic field spectra in the Hamada coordinates in the plasma periphery. However, it should be noted that the fixed boundary version of the VMEC is applied in this paper, and therefore, the shape of the plasma periphery is unchanged even in finite beta equilibria. The HINT code calculation shows the possibility of magnetic surface breaking around the plasma periphery due to the finite pressure in $L = 2$ heliotron/torsatrons [26]. In these cases, the determination of plasma periphery where this model should be applied itself would be a complex

problem, because plasma periphery is significantly unclear due to the superposition of magnetic islands with several toroidal and poloidal mode numbers. The effects of magnetic islands on viscous damping of plasma rotation in the W7-AS has been recently investigated correlated with the limited window of the rotational transform for the L-H transition [27]. It is reported that there is a possibility of the significant enhancement of poloidal viscous damping rate in the neighborhood of magnetic islands. Therefore, more accurate situations should be considered to clarify finite beta effects on poloidal viscosity, which would strongly depend on the experimental observations.

3.2 A Quasi-Axisymmetric (QAS) Stellarator

The quasi-axisymmetric configurations have been considered for the improvement of energetic particle confinement with realizing the magnetic configuration with a symmetry [11]. Some MHD analyses on QAS configurations and the effects of the bootstrap current on MHD properties have been studied [14] to improve this concept further.

One another attractive aspect of the QAS configuration would be maintaining of the plasma rotation to suppress the anomalous transport due to the plasma flow velocity shear. The QAS configuration is typically discussed based on the Boozer coordinates because the guiding center equations in the Boozer coordinates are easily computable with only the knowledge of the magnetic field strength and some magnetic surface quantities. However, there is a possibility to have significantly different magnetic field components between the Boozer and the Hamada coordinates as shown in Fig. 1(b) and (c). If there are some helical components in the Hamada coordinates, the dependence of the poloidal viscosity on the poloidal Mach number may be similar to that in the non-symmetric helical systems, which largely makes the QAS configurations less attractive. Therefore, it is essential to examine that QAS configurations in the Boozer coordinates have QAS properties even in the Hamada coordinates or not to consider the poloidal rotation properties.

Figure 6 shows the normalized poloidal viscosity as a function of poloidal Mach number for a reference QAS configuration described in Ref. [14]. The result demonstrates that helicities are well suppressed or QAS properties are well maintained even in the Hamada coordinates. This is probably due to the suppressed helicities in the Boozer coordinates, which contribute to the mode coupling very little in the transformation to the Hamada coordinates. Therefore, the bifurcation of the poloidal Mach number can be anticipated in QAS configurations as observed during the L-H transition in many tokamaks, which would make the QAS concept more attractive for proceeding to the

real experiments.

3.3 A Quasi-Helically Symmetric (QHS) Stellarator

Finally, a QHS configuration is mentioned. The equation (2) is obtained by using the relation that the geometrical inverse aspect ratio is almost comparable to the toroidicity in the magnetic field [28], which is not the case for QHS configurations. Thus, more accurately, the expression of the poloidal viscosity which is appropriate for QHS configurations should be derived. However, the main purpose to consider QHS configurations here is to grasp the effects of magnetic field spectrum control on the poloidal viscosity, and therefore, the eq. (2) is applied. The example QHS configuration is obtained through the plasma boundary modulations with $M = 5$ [29].

Analogous to QAS configurations, the example QHS configuration maintains QHS properties even in the Hamada coordinates due to the significantly weak mode coupling in the coordinate transformation. Therefore, the example QHS configuration has one clear local maximum around $M_p \gtrsim |m - nq|/m$ (about 2.8 for this case), which is clearly shown in Fig. 7. It is noted that the weak local maximum also appears around $M_p \sim 1$, however; this is due to the above mentioned approximation, and thus, the value of $\Pi_{p,n}$ is much smaller than the TM arising from the toroidicity in the magnetic field (cf., Fig. 6). It should be also noted that the value of $\Pi_{p,n}$ for the HM is $|m - nq|$ times smaller than that for the TM if $\epsilon_{1,0}$ and $\epsilon_{m,n}$ are almost the same. This is due to the factor $m/(m - nq)$ appearing in eq. (2).

The HSX device [13] is also a QHS configuration with the dominant helicity with $(m, n) = (1, 4)$. The poloidal viscosity as a function of M_p was calculated in Ref. [30], which makes the single clear HM around $M_p \sim 4$. The magnetic field spectra in the Boozer coordinates are utilized for this calculation, however; as mentioned above, the result would be qualitatively unchanged even if the magnetic field spectra in the Hamada coordinates are employed.

4 Summary

The nonlinear poloidal viscosity in the plasma periphery has been evaluated for the $L = 2$ LHD-like heliotron and quasi-axisymmetric (QS) stellarators, which indicates the possibility of occurenece of the L-H transition. When the poloidal viscosity as a function of the poloidal Mach number M_p has a local maximum, poloidal Mach number has a possibility to bifurcate from lower M_p (L mode) to higher M_p (H mode). The

appearance of local maxima depends on the relative amplitudes between toroidicity and helicities in the magnetic field.

In the LHD standard-like configuration, Fourier spectra of the magnetic field strength $|B|$ in the Hamada coordinates are significantly different from those in the Boozer coordinates. The dominant helicity in the Boozer coordinates with the same poloidal and toroidal mode numbers as the $L = 2$ helical coil windings is converted to its satellites due to the mode coupling in the coordinate transformation. These helicities cause their local maxima around $M_p \gtrsim |m - nq|/m$, where m (n) detotes the poloidal (toroidal) mode number and q the safety factor. These helicity induced local maxima (HM) shade the toroidicity induced local maxima (TM) occuring around $M_p \gtrsim 1$, which would make difficult to realize the bifurcation of M_p in the appropriate Mach number.

Effects of magnetic configuration control on the poloidal viscosity are also investigated to approach the favorable properties from the viewpoints of poloidal rotation in the LHD-like $L = 2$ heliotron. The less inward magnetic axis shift at zero beta is attractive for the possibility of the bifurcation of the poloidal flow velocity. The quadrupole induced horizontally elongation of the magnetic surface cross sections effectively decreases $\Pi_{p,n}$ to maintain the poloidal flow velocity. However; these magnetic configurations have degraded properties on the particle orbit confinement compared to the LHD standard-like configuration. Therefore, compatibility between these properties should be explored based on the investigations of the relationships between magnetic configuration control and magnetic field spectra. The magnetic field spectra in the Hamada coordinates often deviate from those in the Boozer coordinates, and are difficult to consider intuitively. Therefore, it would be helpful to derivate the expression for the poloidal viscosity in the Boozer coordinates to grasp the effects of magnetic configuration control on the poloidal rotation properties.

QS configurations are also examined because the maintaining of the plasma rotation is considered as the one of the attractions for QS concepts. The QS properties are typically discussed in the Boozer coordinates from the particle orbit point of views. The QS properties in the Boozer coordinates are well maintained even in the Hamada coordinates. This is due to the well suppressed non-symmetric magnetic field spectra in the Boozer coordinates, which causes very little mode coupling in the coordinate transformation to the Hamada coordinates. Therefore, TM (HM) appears sufficiently clearly in an example QAS (QHS) configuration, which implies that there is a possibility of the bifurcation of the poloidal flow velocity in the appropriate Mach number.

These clear local maxima appearing around different M_p ($M_p \sim 2$ (4) for an example

QAS (QHS) configuration) and the variation of the dependence of poloidal viscosity on M_p possible by the magnetic configuration control in LHD-like $L = 2$ heliotron would provide the good opportunity to test this bifurcation model in a wide range.

Acknowledgements

The authors gratefully acknowledge for productive discussions with Prof. M. Wakatani.

References

[1] GROEBNER, R. J., et al., Phys. Rev. Lett. **64**(1990)3015.

[2] IDA, K., et al., Phys. Rev. Lett. **65**(1990)1364.

[3] SHAING, K. C., CRUME, E. C. Jr., Phys. Rev. Lett. **63**(1989) 2369.

[4] ITOH, K., ITOH, S. -I., Nucl. Fusion **32**(1992)2243.

[5] TAYLOR, R. J., Phys. Rev. Lett. **63**(1989)2365.

[6] WEYNANTS, R. R., TAYLOR, R. J., Nucl. Fusion **30**(1990)945.

[7] SHAING, K. C., Phys. Fluids **B5**(1993)3841.

[8] YOKOYAMA. M., WAKATANI. M., SHAING, K. C., Nucl. Fusion **35**(1995)153.

[9] IIYOSHI, A., et al., Fusion Technol. **17**(1990)169.

[10] NÜHRENBERG, J., ZILLE, R., Phys. Lett. **A129**(1988)113.

[11] NÜHRENBERG, J., in Theory of Fusion Plasmas (Proc. Workshop Varenna, 1994) Editrice Compositori, Bologna (1994)3.

[12] GARABEDIAN, P., Phys. Plasmas **3**(1996)2483.

[13] ANDERSON, D. T., et al., HSX — A Helically Symmetric Toroidal Experiment — (edited by Torsatron/Stellarator Laboratory, Univ. of Wisconsin-Madison) (1993).

[14] NAKAJIMA, N., YOKOYAMA, M., OKAMOTO, M., NÜHRENBERG, J., Plasma Phys. Reports **23**(1997)460.

[15] REIMAN, A. H., et al., Plasma Phys. Reports **23**(1997)472.

[16] HAMADA, S., Nucl. Fusion **2**(1962)23.

[17] CORONADO, M., GALINDO TREJO, J., Phys. Fluids **B2**(1990)530.

[18] HIRSHMAN, S. P., et al., Comput. Phys. Commun. **43**(1986)143.

[19] NISHIMURA, K., et al., Fusion Technol. **17**(1990)86.

[20] BOOZER, A. H., Phys. Fluids **23**(1980)904.

[21] NAKAJIMA, N., TODOROKI, J., OKAMOTO, M., kakuyugo-kenkyu **68**(1992)395.

[22] ICHIGUCHI, K., NAKAJIMA, N., OKAMOTO, M., Nucl. Fusion **37**(1997)1109.

[23] ICHIGUCHI, K., MOTOJIMA, O., YAMAZAKI, K., NAKAJIMA, N., OKAMOTO, M., Nucl. Fusion **36**(1996)1145.

[24] TODOROKI, J., et al., in Proc. 12th Int. Conf. on Plasma Physics and Controlled Nuclear Fusion Research, 1988, Nice (Vienna 1989) Vol.2, p.637.

[25] SHAING, K. C., Phys. Fluids **B5**(1993)3841.

[26] HAYASHI, T., TAKEI, A., SATO, T., Phys. Fluids **B4**(1992)1539.

[27] WOBIG, H., KIβLINGER, J., "The Effect of Magnetic Field Geometry on Viscous Damping of Rotation in Stellarators", IPP2/334, Max-Planck-Institut für Plasmaphysik, EURATOM-Association (1997).

[28] CORONADO, M., TALMADGE, J. N., Phys. Fluids **B5**(1993)1200.

[29] YOKOYAMA, M., NAKAJIMA, N., OKAMOTO, M., submitted to Nucl. Fusion.

[30] TALMADGE, J. N., et al., in Plasma Physics and Controlled Nuclear Fusion Research 1994 (Proc. 15th Int. Conf. Seville, 1994), Vol.1, IAEA, Vienna (1995)797.

Δ cm						
0	$(\epsilon_{1,0})$ 0.159	$(\epsilon_{4,10})$ 0.093	$(\epsilon_{0,-10})$ 0.088	$(\epsilon_{1,-10})$ 0.068	$(\epsilon_{2,10})$ 0.065	$(\epsilon_{5,10})$ 0.064
-15	$(\epsilon_{1,10})$ 0.139	$(\epsilon_{3,10})$ 0.128	$(\epsilon_{1,0})$ 0.123	$(\epsilon_{0,10})$ 0.118	$(\epsilon_{1,-10})$ 0.061	$(\epsilon_{4,10})$ 0.059
-30	$(\epsilon_{2.10})$ 0.202	$(\epsilon_{1,10})$ 0.148	$(\epsilon_{0,-10})$ 0.061	$(\epsilon_{3.20})$ 0.060	$(\epsilon_{1,0})$ 0.057	$(\epsilon_{3,10})$ 0.051

Table. I Dominant magnetic field spectra in the Hamada coordinates for three vacuum configurations with different inward magnetic axis shift Δ.

Horizontal, $\Delta = -13$ cm	$(\epsilon_{1,0})$ 0.120	$(\epsilon_{0,-10})$ 0.086	$(\epsilon_{1,-10})$ 0.073	$(\epsilon_{4,10})$ 0.067	$(\epsilon_{1,10})$ 0.061
Vertical, $\Delta = -16$ cm	$(\epsilon_{3,10})$ 0.133	$(\epsilon_{0,-10})$ -0.103	$(\epsilon_{1,0})$ 0.102	$(\epsilon_{1,10})$ 0.099	$(\epsilon_{1,-10})$ 0.057

Table. II Dominant magnetic field spectra in the Hamada coordinates for the configuration with $\Delta = -13$ cm with the horizontally elongated magnetic surface cross sections in the toroidal average.

Figure Captions

Fig. 1: **(a)** Poincaré plots of magnetic field lines at $\phi = 0, (1/4)(2\pi/10)$ and $(1/2)(2\pi/10)$ from left to right, respectively, for the LHD standard-like configuration. **(b)** Fourier spectra of the magnetic field strength in the Boozer coordinates for the configuration shown in Fig. 1(a). The m (n) denotes the poloidal (toroidal) mode number, respectively. **(c)** Fourier spactra of the magnetic field strength in the Hamada coordinates for the configurations shown in Fig. 1(a).

Fig. 2: Normalized poloidal viscosity $\Pi_{p,n}$ versus poloidal Mach number M_p for the LHD standard-like configuration shown in Fig. 1(a). The results for $(\nu_{*i}, \nu_{eff}/(v_T/Rq)) = (1, 0.01), (1, 0.1)$ and (12, 0.01) cases are shown.

Fig. 3: $\Pi_{p,n}$ versus M_p for three vacuum configurations with diffrent values of inward magnetic axis shift, Δ.

Fig. 4: **(a)** Poincaré plots of magnetic field lines at $\phi = 0, (1/4)(2\pi/10)$ and $(1/2)(2\pi/10)$ from left to right, respectively, for the horizontally elongated magnetic surface cross sections due to the quadrupole field control in LHD-like coil system. **(b)** $\Pi_{p,n}$ versus M_p for the configuration shown in Fig. 4(a). For reference, the results for the LHD standard-like configuration and vertically elongated case with $\Delta = -16$ cm are also shown.

Fig. 5: $\Pi_{p,n}$ versus M_p for finite beta cases in the LHD standard-like configuration.

Fig. 6: $\Pi_{p,n}$ versus M_p for a reference QAS configuration [14].

Fig. 7: $\Pi_{p,n}$ versus M_p for an example QHS configuration [29].

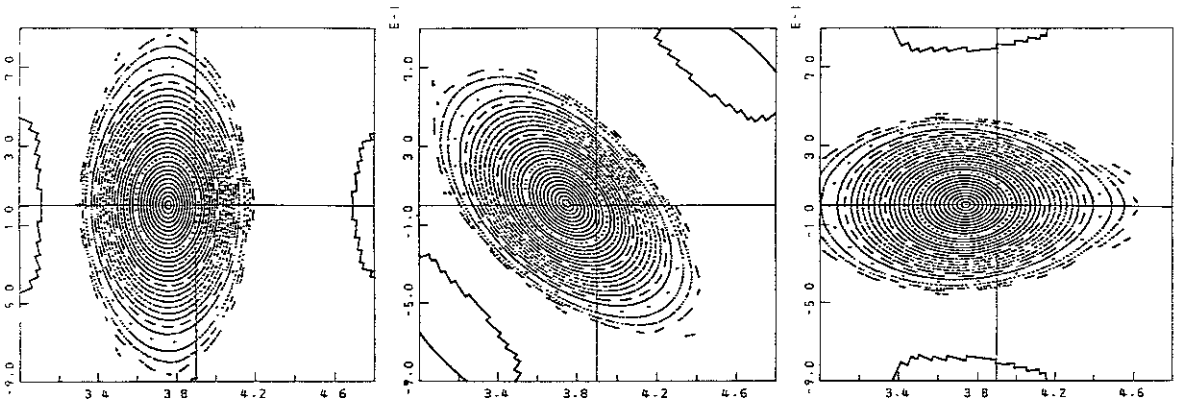

Fig. 1(a)

< Spectrum of B(Boozer) in full mesh>

$B = \Sigma B_{(m,n)}\cos[m\vartheta - n\zeta]$

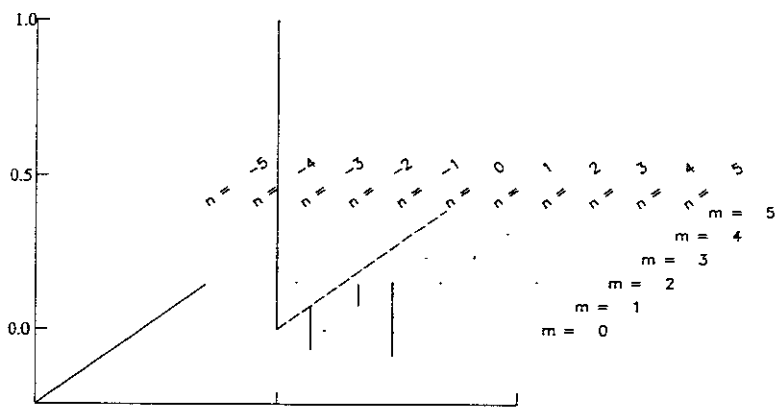

Fig. 1(b)

< Spectrum of B(Hamada) in full mesh>

$B = \Sigma B_{(m,n)}\cos[m\vartheta - n\zeta]$: $\max|B_H/B_B - 1| =$ 2.12427E-03 %

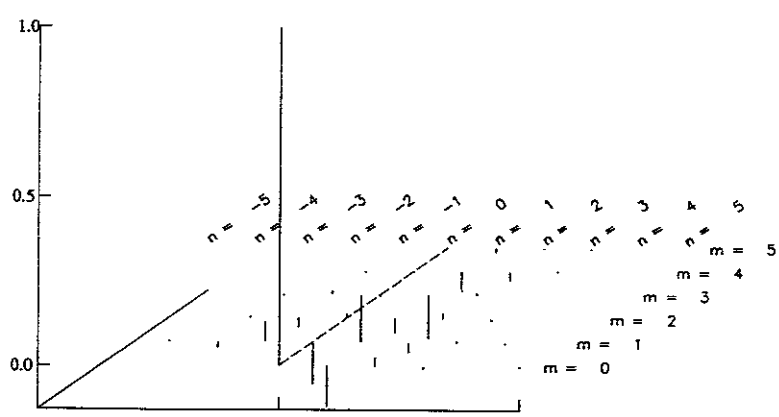

Fig. 1(c)

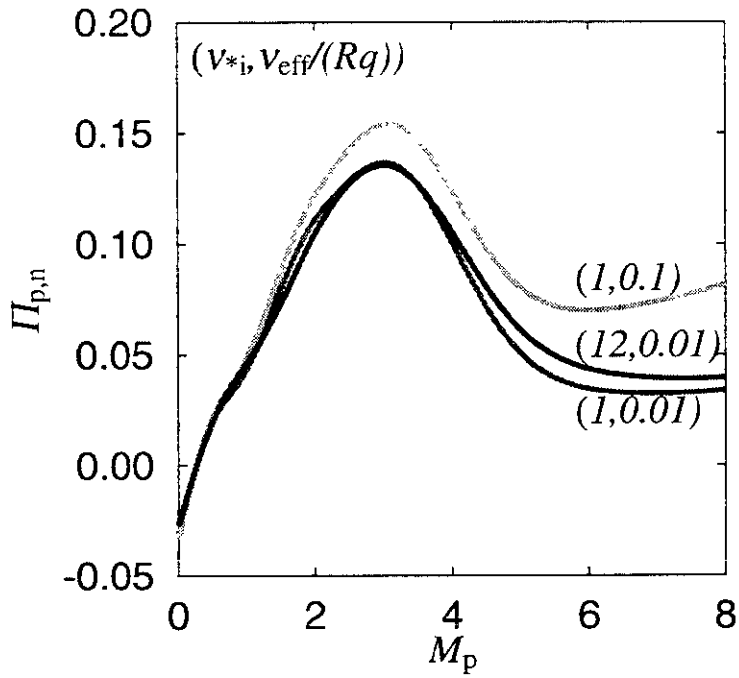
0.20
0.15
0.10
0.05
0.00
-0.05
0
2
4
6
8
$(\nu_{*i}, \nu_{eff}/(Rq))$
(1,0.1)
(12,0.01)
(1,0.01)
$\Pi_{p,n}$
M_p

Fig. 2

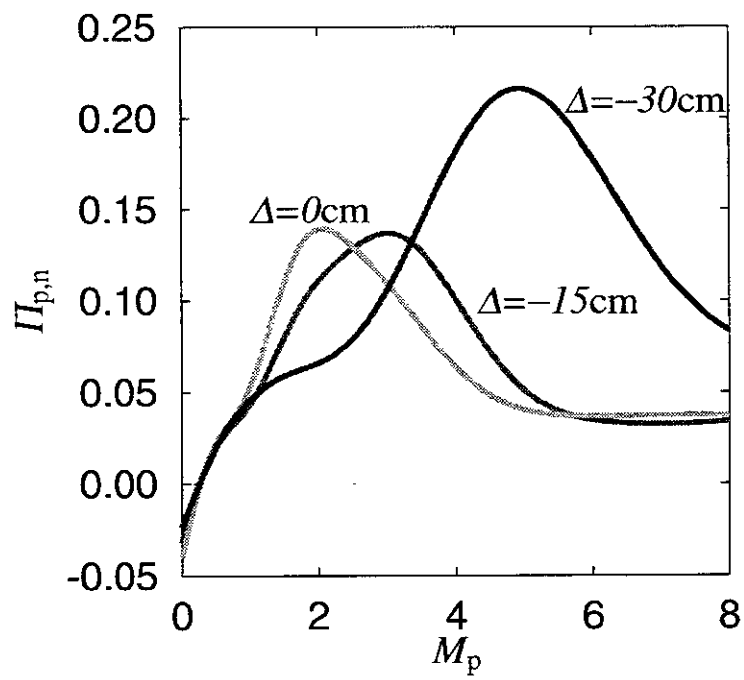
0.25
0.20
0.15
0.10
0.05
0.00
-0.05
0
2
4
6
8
Δ=−30cm
Δ=0cm
Δ=−15cm
$\Pi_{p,n}$
M_p

Fig. 3

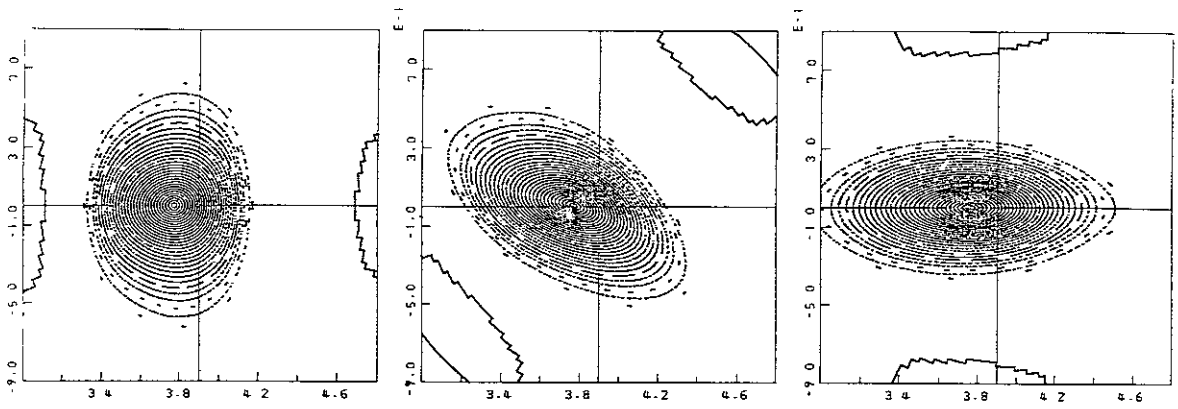

Fig. 4(a)

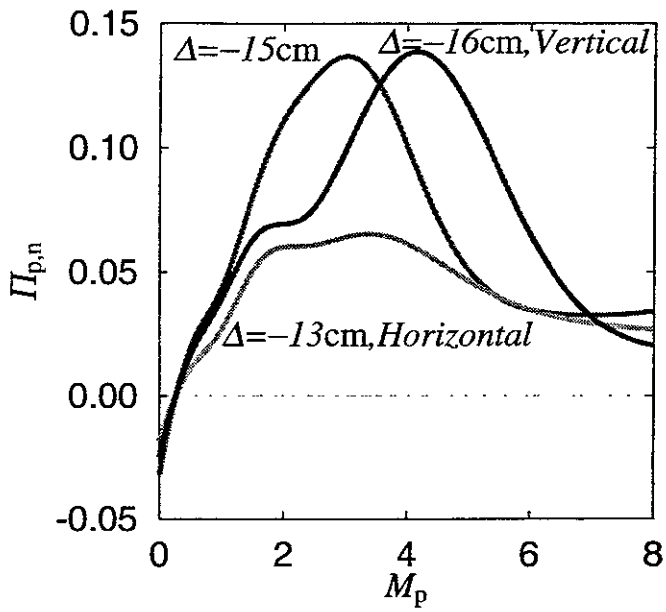

Fig. 4(b)

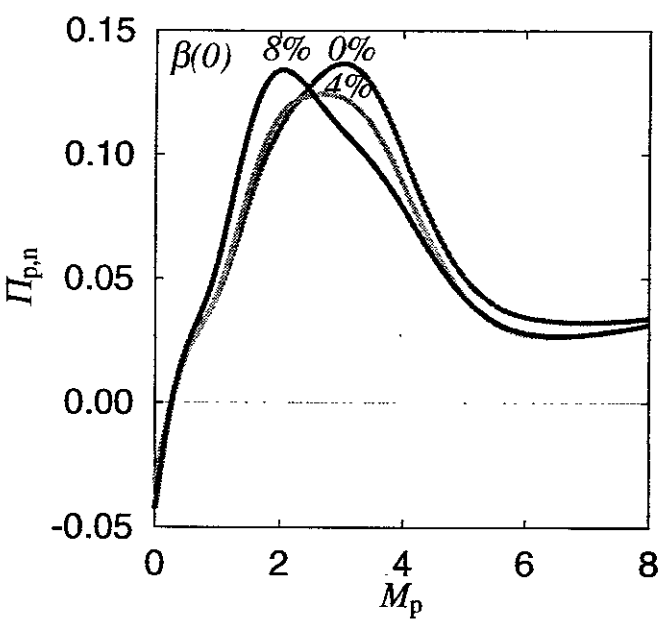

Fig. 5

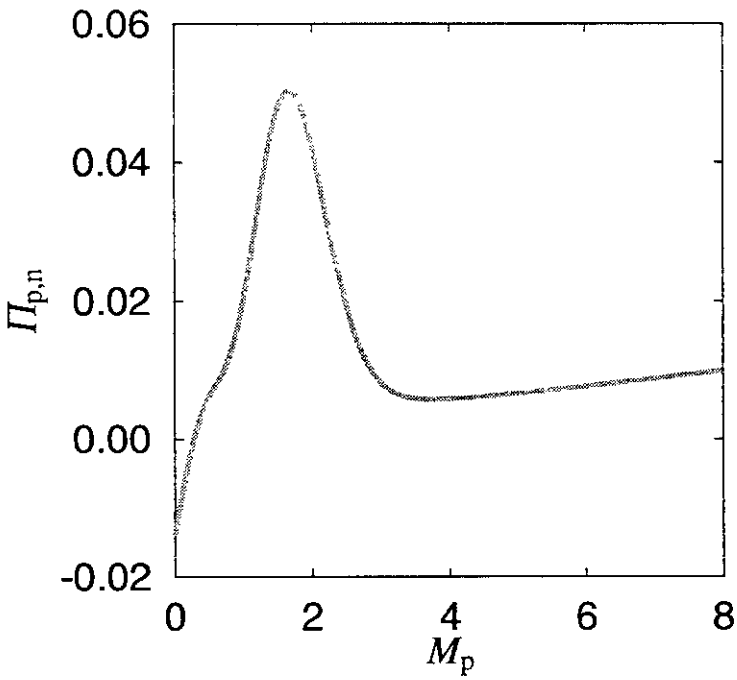
0.06
0.04
0.02
0.00
-0.02
$\Pi_{p,n}$
0
2
4
6
8
M_p

Fig. 6

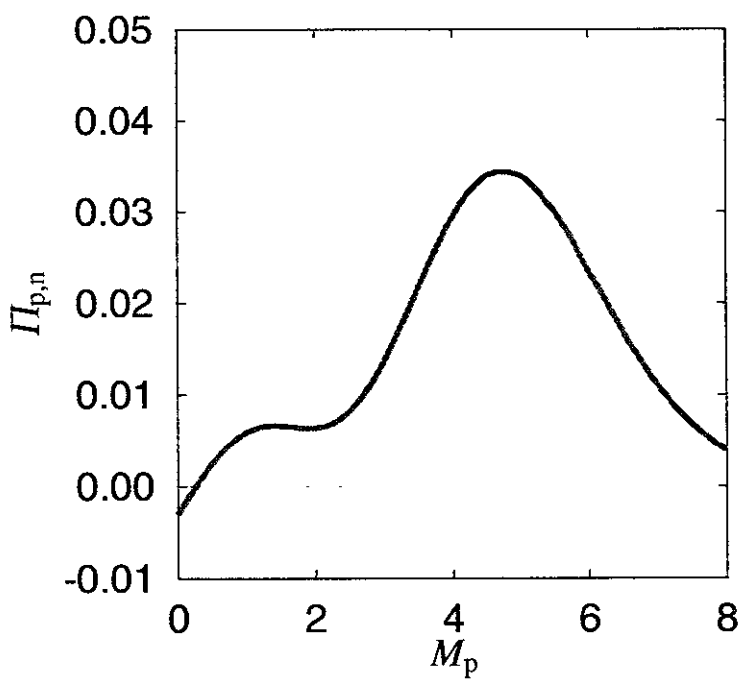
0.05
0.04
0.03
0.02
0.01
0.00
-0.01
$\Pi_{p,n}$
0
2
4
6
8
M_p

Fig. 7

Recent Issues of NIFS Series

NIFS-471 A. Fujisawa, H. Iguchi, S. Lee and Y. Hamada,
Effects of Horizontal Injection Angle Displacements on Energy Measurements with Parallel Plate Energy Analyzer; Dec. 1996

NIFS-472 R. Kanno, N. Nakajima, H. Sugama, M. Okamoto and Y. Ogawa,
Effects of Finite-β and Radial Electric Fields on Neoclassical Transport in the Large Helical Device; Jan. 1997

NIFS-473 S. Murakami, N. Nakajima, U. Gasparino and M. Okamoto,
Simulation Study of Radial Electric Field in CHS and LHD; Jan. 1997

NIFS-474 K. Ohkubo, S. Kubo, H. Idei, M. Sato, T. Shimozuma and Y. Takita,
Coupling of Tilting Gaussian Beam with Hybrid Mode in the Corrugated Waveguide; Jan. 1997

NIFS-475 A. Fujisawa, H. Iguchi, S. Lee and Y. Hamada,
Consideration of Fluctuation in Secondary Beam Intensity of Heavy Ion Beam Prove Measurements; Jan. 1997

NIFS-476 Y. Takeiri, M. Osakabe, Y. Oka, K. Tsumori, O. Kaneko, T. Takanashi, E. Asano, T. Kawamoto, R. Akiyama and T. Kuroda,
Long-pulse Operation of a Cesium-Seeded High-Current Large Negative Ion Source; Jan. 1997

NIFS-477 H. Kuramoto, K. Toi, N. Haraki, K. Sato, J. Xu, A. Ejiri, K. Narihara, T. Seki, S. Ohdachi, K. Adati, R. Akiyama, Y. Hamada, S. Hirokura, K. Kawahata and M. Kojima,
Study of Toroidal Current Penetration during Current Ramp in JIPP T-IIU with Fast Response Zeeman Polarimeter; Jan., 1997

NIFS-478 H. Sugama and W. Horton,
Neoclassical Electron and Ion Transport in Toroidally Rotating Plasmas; Jan. 1997

NIFS-479 V.L. Vdovin and I.V. Kamenskij,
3D Electromagnetic Theory of ICRF Multi Port Multi Loop Antenna; Jan. 1997

NIFS-480 W.X. Wang, M. Okamoto, N. Nakajima, S Murakami and N. Ohyabu,
Cooling Effect of Secondary Electrons in the High Temperature Divertor Operation; Feb. 1997

NIFS-481 K. Itoh, S.-I. Itoh, H. Soltwisch and H.R. Koslowski,
Generation of Toroidal Current Sheet at Sawtooth Crash; Feb. 1997

NIFS-482 K. Ichiguchi,
Collisionality Dependence of Mercier Stability in LHD Equilibria with Bootstrap Currents; Feb. 1997

NIFS-483 S. Fujiwara and T. Sato,
Molecular Dynamics Simulations of Structural Formation of a Single Polymer Chain: Bond-orientational Order and Conformational Defects; Feb. 1997

NIFS-484 T. Ohkawa,
Reduction of Turbulence by Sheared Toroidal Flow on a Flux Surface; Feb. 1997

NIFS-485 K. Narihara, K. Toi, Y. Hamada, K. Yamauchi, K. Adachi, I. Yamada, K. N. Sato, K. Kawahata, A. Nishizawa, S. Ohdachi, K. Sato, T. Seki, T. Watari, J. Xu, A. Ejiri, S. Hirokura, K. Ida, Y. Kawasumi, M. Kojima, H. Sakakita, T. Ido, K. Kitachi, J. Koog and H. Kuramoto,
Observation of Dusts by Laser Scattering Method in theJIPPT-IIU Tokamak Mar. 1997

NIFS-486 S. Bazdenkov, T. Sato and The Complexity Simulation Group,
Topological Transformations in Isolated Straight Magnetic Flux Tube; Mar. 1997

NIFS-487 M. Okamoto,
Configuration Studies of LHD Plasmas; Mar. 1997

NIFS-488 A. Fujisawa, H. Iguchi, H. Sanuki, K. Itoh, S. Lee, Y. Hamada, S. Kubo, H. Idei, R. Akiyama, K. Tanaka, T. Minami, K. Ida, S. Nishimura, S. Morita, M. Kojima, S. Hidekuma, S.-I. Itoh, C. Takahashi, N. Inoue, H. Suzuki, S. Okamura and K. Matsuoka,
Dynamic Behavior of Potential in the Plasma Core of the CHS Heliotron/Torsatron; Apr. 1997

NIFS-489 T. Ohkawa,
Pfirsch - Schlüter Diffusion with Anisotropic and Nonuniform Superthermal Ion Pressure; Apr. 1997

NIFS-490 S. Ishiguro and The Complexity Simulation Group,
Formation of Wave-front Pattern Accompanied by Current-driven Electrostatic Ion-cyclotron Instabilities; Apr. 1997

NIFS-491 A. Ejiri, K. Shinohara and K. Kawahata,
An Algorithm to Remove Fringe Jumps and its Application to Microwave Reflectometry; Apr. 1997

NIFS-492 K. Ichiguchi, N. Nakajima, M. Okamoto,
Bootstrap Current in the Large Helical Device with Unbalanced Helical Coil Currents; Apr. 1997

NIFS-493 S. Ishiguro, T. Sato, H. Takamaru and The Complexity Simulation Group,
V-shaped dc Potential Structure Caused by Current-driven Electrostatic Ion-cyclotron Instability; May 1997

NIFS-494 K. Nishimura, R. Horiuchi, T. Sato,
Tilt Stabilization by Energetic Ions Crossing Magnetic Separatrix in Field-Reversed Configuration; June 1997

NIFS-495 T. -H. Watanabe and T. Sato,
Magnetohydrodynamic Approach to the Feedback Instability; July 1997

NIFS-496 K. Itoh, T. Ohkawa, S. -I.Itoh, M. Yagi and A. Fukuyama
Suppression of Plasma Turbulence by Asymmetric Superthermal Ions; July 1997

NIFS-497 T. Takahashi, Y. Tomita, H. Momota and Nikita V. Shabrov,
Collisionless Pitch Angle Scattering of Plasma Ions at the Edge Region of an FRC; July 1997

NIFS-498 M. Tanaka, A.Yu Grosberg, V.S. Pande and T. Tanaka,
Molecular Dynamics and Structure Organization in Strongly-Coupled Chain of Charged Particles; July 1997

NIFS-499 S. Goto and S. Kida,
Direct-interaction Approximation and Reynolds-number Reversed Expansion for a Dynamical System; July 1997

NIFS-500 K. Tsuzuki, N. Inoue, A. Sagara, N. Noda, O. Motojima, T. Mochizuki, T. Hino and T. Yamashina,
Dynamic Behavior of Hydrogen Atoms with a Boronized Wall; July 1997

NIFS-501 I. Viniar and S. Sudo,
Multibarrel Repetitive Injector with a Porous Pellet Formation Unit; July 1997

NIFS-502 V. Vdovin, T. Watari and A. Fukuyama,
An Option of ICRF Ion Heating Scenario in Large Helical Device; July 1997

NIFS-503 E. Segre and S. Kida,
Late States of Incompressible 2D Decaying Vorticity Fields; Aug. 1997

NIFS-504 S. Fujiwara and T. Sato,
Molecular Dynamics Simulation of Structural Formation of Short Polymer Chains; Aug. 1997

NIFS-505 S. Bazdenkov and T. Sato
Low-Dimensional Model of Resistive Interchange Convection in Magnetized Plasmas; Sep. 1997

NIFS-506 H. Kitauchi and S. Kida,
Intensification of Magnetic Field by Concentrate-and-Stretch of Magnetic Flux Lines; Sep. 1997

NIFS-507 R.L. Dewar,
Reduced form of MHD Lagrangian for Ballooning Modes; Sep. 1997

NIFS-508 Y.-N. Nejoh,
Dynamics of the Dust Charging on Electrostatic Waves in a Dusty Plasma with Trapped Electrons; Sep.1997

NIFS-509 E. Matsunaga, T.Yabe and M. Tajima,
Baroclinic Vortex Generation by a Comet Shoemaker-Levy 9 Impact; Sep. 1997

NIFS-510 C.C. Hegna and N. Nakajima,
On the Stability of Mercier and Ballooning Modes in Stellarator Configurations; Oct. 1997

NIFS-511 K. Orito and T. Hatori,
Rotation and Oscillation of Nonlinear Dipole Vortex in the Drift-Unstable Plasma; Oct. 1997

NIFS-512 J. Uramoto,
Clear Detection of Negative Pionlike Particles from H_2 Gas Discharge in Magnetic Field; Oct. 1997

NIFS-513 T. Shimozuma, M. Sato, Y. Takita, S. Ito, S. Kubo, H. Idei, K. Ohkubo, T. Watari, T.S. Chu, K. Felch, P. Cahalan and C.M. Loring, Jr,
The First Preliminary Experiments on an 84 GHz Gyrotron with a Single-Stage Depressed Collector; Oct. 1997

NIFS-514 T. Shjmozuma, S. Morimoto, M. Sato, Y. Takita, S. Ito, S. Kubo, H. Idei, K. Ohkubo and T. Watari,
A Forced Gas-Cooled Single-Disk Window Using Silicon Nitride Composite for High Power CW Millimeter Waves; Oct. 1997

NIFS-515 K. Akaishi,
On the Solution of the Outgassing Equation for the Pump-down of an Unbaked Vacuum System; Oct. 1997

NIFS-516 *Papers Presented at the 6th H-mode Workshop (Seeon, Germany)*; Oct. 1997

NIFS-517 John L. Johnson,
The Quest for Fusion Energy; Oct. 1997

NIFS-518 J. Chen, N. Nakajima and M. Okamoto,
Shift-and-Inverse Lanczos Algorithm for Ideal MHD Stability Analysis; Nov. 1997

NIFS-519 M. Yokoyama, N. Nakajima and M. Okamoto,
Nonlinear Incompressible Poloidal Viscosity in L=2 Heliotron and Quasi-Symmetric Stellarators; Nov. 1997